Frequency moments of the spectral density of an atomic-displacement time-correlation function of a three-dimensional Lennard-Jones crystal in the classical and quantum regimes

A. Macchi and A. A. Maradudin
Department of Physics, University of California, Irvine, California 92717

V. Tognetti
Dipartimento di Fisica dell'Universita' di Firenze, Largo Enrico Fermi 2, I-50125 Firenze, Italy
(Received 31 January 1995)

We present a detailed description of the path-integral quantum Monte Carlo and effective potential methods for the calculation of the first few even-frequency moments (up to the fourth) of the spectral density of an atomic-displacement time-correlation function as functions of temperature in the quantum regime. Classical moments are also calculated up to the sixth to analyze the influence of finite-size effects. Numerical results are presented for Lennard-Jones interaction-potential models of solid argon and solid krypton. The relevance of quantum effects at lower temperatures is pointed out. The advantages and limitations of these approaches to the calculation of frequency moments are discussed.

I. INTRODUCTION

The calculation of equilibrium thermodynamics functions of anharmonic crystals in the regime of low temperatures when quantum effects are large can now be carried out with good accuracy by the path-integral quantum Monte Carlo method[1–3] or by the variational effective potential method.[4–6] However, the calculation of nonequilibrium properties of anharmonic crystals in the low-temperature limit, such as time-displaced correlation functions of the atomic displacements, remains a challenging problem.

An approach to solving this problem that has been succesful in application to linear chains is based on working with the spectral density of a time-displaced correlation function, i.e., with the Fourier transform in space and time of such a correlation function.[7] These spectral densities are often measured directly when an external probe, such as a neutron, is scattered by the vibrations of the crystal. In this approach the first few frequency moments of the spectral density are calculated as functions of temperature for a fixed value of the wave vector appearing in the definition of the spectral densities. The calculation of each moment is a calculation of an equilibrium property of the crystal, and can be carried out by the path-integral quantum Monte Carlo method, or by the effective potential method. The spectral density, as a function of frequency, is then reconstructed from these moments, e.g., by a continued fraction representation with a suitable termination.[8–10] If the spectral density consists of a single peak, an accurate determination of it in this way by the use of only few moments is feasible. If the time-displaced correlation function is that of atomic displacements, the peak in the spectral density is centered at the frequency of the phonon whose wave vector is the one for which the spectral density has been calculated, and its width gives the inverse lifetime of that phonon due to its interactions with the other phonons of the crystal. Thus, from calculations of such spectral densities the temperature dependence of the phonon frequencies and lifetimes can be determined in a nonperturbative fashion. In view of the success of such calculations of these important characteristics of phonons for one-dimensional crystals,[11,12] it is of interest to explore the possibility of carrying out analogous calculations for three-dimensional, Bravais, crystals. By suitable choices of the components of the atomic displacements entering the correlation function, and by choosing the wave vectors for which the spectral density is being calculated along symmetry directions in the Brillouin zone of the crystal, one can ensure that the resulting spectral density possesses a single peak. It is therefore reasonable to expect that a good representation of the spectral density can be obtained by the use of only a few frequency moments. In this paper we describe the calculation of the temperature dependence of the first few frequency moments of a time-displaced correlation function of atomic displacements for a nearest-neighbor Lennard-Jones (LJ) crystal, i.e., a face-centered-cubic crystal in which each atom interacts only with its 12 nearest neighbors through a 6-12 Lennard-Jones potential. The long-range interactions are taken into account in a static approximation.

The path-integral Monte Carlo and effective potential methods will be used in the calculations, and various tests of the reliability of the results obtained will be carried out. The use of these moments in different approaches to the reconstruction of the spectral density will be described in a subsequent paper.

The outline of this paper is the following. In Sec. II we define the displacement correlation function to be stud-

ied in this paper and obtain formal expressions for the first four even-frequency moments of its spectral density. The evaluation of the quantum mechanical averages that appear in the expressions for the moments on the basis of both the path-integral quantum Monte Carlo and effective potential methods is discussed in Sec. III. In Sec. IV the three-dimensional (3D) Lennard-Jones crystal model underlying the numerical calculations carried out in this paper is introduced, and the Monte Carlo method used in this calculation is described. Numerical results for the frequency moments of the spectral density of atomic displacements as functions of temperature in both the classical and quantum regimes are presented in Secs. V and VI for solid argon and solid krypton. A summary of the results obtained, and the conclusions reached from them, in Sec. VII, concludes the paper.

II. DISPLACEMENT CORRELATION FUNCTION OF A 3D CRYSTAL

Let us consider a crystal of N atoms of mass m moving in three dimensions and interacting through a pairwise central potential $u(r)$. Its Hamiltonian is

$$\hat{H} = \sum_{\mathbf{l}} \frac{\hat{\mathbf{p}}_{\mathbf{l}}^2}{2m} + V(\hat{\mathbf{X}}), \tag{1}$$

where

$$V(\hat{\mathbf{X}}) = \frac{1}{2} \sum_{\mathbf{l}} \sum_{n} \sum_{\mathbf{d}_n} u\left(|\hat{\mathbf{x}}_{\mathbf{l}+\mathbf{d}_n} - \hat{\mathbf{x}}_{\mathbf{l}}|\right). \tag{2}$$

In Eqs. (1) and (2) atoms have been labeled by their classical equilibrium position $\mathbf{l} \equiv \{\mathbf{l}_\alpha\}(\alpha = 1,2,3)$ corresponding to the sites of a fcc Bravais lattice, $\hat{\mathbf{p}}_{\mathbf{l}} \equiv \{\hat{p}_{\mathbf{l}\alpha}\}$ and $\hat{\mathbf{x}}_{\mathbf{l}} \equiv \{\hat{x}_{\mathbf{l}\alpha}\}$ are the instantaneous momentum and position operators of the lth atom, and the sum over $n = 1,2,\ldots$ takes into account its interaction with the successive shells of neighbors labeled by their relative equilibrium position $\mathbf{d}_n$. The dynamical behavior of the system is investigated by means of the symmetrized spectral density tensor

$$C_{\alpha\beta}(\mathbf{k},\omega) = \frac{1}{4\pi} \int dt e^{i\omega t} \langle \hat{\xi}_{\mathbf{k},\alpha}(t)\hat{\xi}_{-\mathbf{k},\beta}(0) + \hat{\xi}_{-\mathbf{k},\beta}(0)\hat{\xi}_{\mathbf{k},\alpha}(t)\rangle, \tag{3}$$

where the $\mathbf{k}$ vector is defined within the first Brillouin zone (FBZ), and

$$\hat{\boldsymbol{\xi}}_{\mathbf{k}} = \frac{1}{\sqrt{N}} \sum_{\mathbf{l}} e^{i\mathbf{k}\cdot\mathbf{l}} \hat{\boldsymbol{\xi}}_{\mathbf{l}} \tag{4}$$

is the Fourier transform in $\mathbf{k}$ space of $\hat{\boldsymbol{\xi}}_{\mathbf{l}} = \hat{\mathbf{x}}_{\mathbf{l}} - \mathbf{l}$, i.e., of the instantaneous displacement of the lth atom from its classical equilibrium position. Moreover, the angular brackets stand for the canonical average

$$\langle \hat{A} \rangle = \frac{1}{Z} \mathrm{Tr}(\hat{\rho}\hat{A}), \tag{5}$$

where $Z = \mathrm{Tr}(\hat{\rho})$ is the partition function and $\hat{\rho} = \exp(-\beta\hat{H})$ is the non-normalized density matrix. It is convenient to introduce the projections of $C_{\alpha\beta}(\mathbf{k},\omega)$ along the longitudinal and transverse polarizations of the vibrational mode $\mathbf{k}$, namely,

$$C_\mu(\mathbf{k},\omega) = \sum_{\alpha\beta} \epsilon_{\mathbf{k}\mu,\alpha} C_{\alpha\beta}(\mathbf{k},\omega) \epsilon_{\mathbf{k}\mu,\beta}, \tag{6}$$

where $\epsilon_{\mathbf{k}\mu}$ $(\mu = 1,2,3)$ are the polarization vectors. By expressing the thermal average in square brackets in terms of the exact eigenfunctions and eigenvalues of the Hamiltonian $\hat{H}$ it can be proved that $C_\mu(\mathbf{k},\omega)$ possesses the symmetry properties

$$C_\mu(\mathbf{k},\omega) = C_\mu(-\mathbf{k},-\omega) = C_\mu(\mathbf{k},-\omega) = C_\mu(-\mathbf{k},\omega), \tag{7}$$

where we have also used the fact that every atom in the lattice is at a center of inversion symmetry. The even-frequency moments of $C_\mu(\mathbf{k},\omega)$ are defined by

$$M_{2n,\mu}(\mathbf{k}) = \int d\omega C_\mu(\mathbf{k},\omega)\omega^{2n}, \tag{8}$$

while the odd moments vanish in view of Eq. (7). By combining Eqs. (8) and (6), and taking advantage of the stationary properties of the system, the expressions for the frequency moments can be written in a very convenient way as follows:

$$M_{2n,\mu}(\mathbf{k}) = \frac{1}{2} \left\langle \left(\boldsymbol{\epsilon}_{\mathbf{k}\mu} \cdot \hat{\boldsymbol{\xi}}_{\mathbf{k}}^{(n)}\right)\left(\boldsymbol{\epsilon}_{\mathbf{k}\mu} \cdot \hat{\boldsymbol{\xi}}_{-\mathbf{k}}^{(n)}\right) + \left(\boldsymbol{\epsilon}_{\mathbf{k}\mu} \cdot \hat{\boldsymbol{\xi}}_{-\mathbf{k}}^{(n)}\right)\left(\boldsymbol{\epsilon}_{\mathbf{k}\mu} \cdot \hat{\boldsymbol{\xi}}_{\mathbf{k}}^{(n)}\right)\right\rangle, \tag{9}$$

where

$$\hat{\boldsymbol{\xi}}_{\mathbf{k}}^{(n)} = \frac{1}{\sqrt{N}} \sum_{\mathbf{l}} e^{i\mathbf{k}\cdot\mathbf{l}} \frac{d^n}{dt^n} \hat{\boldsymbol{\xi}}_{\mathbf{l}}(t)|_{t=0}. \tag{10}$$

Moreover, the equal time correlation functions given by Eq. (9) can be explicitly evaluated by means of the the equations of motion; in the quantum regime a repeated use of the Heisenberg equations of motion leads to the following expressions for the first four even moments:

$$M_{0,\mu}(\mathbf{k}) = \left\langle \left(\boldsymbol{\epsilon}_{\mathbf{k}\mu} \cdot \hat{\boldsymbol{\xi}}_{\mathbf{k}}\right)\left(\boldsymbol{\epsilon}_{\mathbf{k}\mu} \cdot \hat{\boldsymbol{\xi}}_{-\mathbf{k}}\right)\right\rangle, \tag{11}$$

$$M_{2,\mu}(\mathbf{k}) = \frac{1}{N}\frac{1}{m^2}\sum_{\mathbf{ll'}} e^{i\mathbf{k}\cdot(\mathbf{l}-\mathbf{l'})}\left\langle(\boldsymbol{\epsilon}_{\mathbf{k}\mu}\cdot\hat{\mathbf{p}}_{\mathbf{l}})\,(\boldsymbol{\epsilon}_{\mathbf{k}\mu}\cdot\hat{\mathbf{p}}_{\mathbf{l'}})\right\rangle$$

$$= \frac{1}{m^2}\left\langle(\boldsymbol{\epsilon}_{\mathbf{k}\mu}\cdot\hat{\mathbf{p}}_{\mathbf{k}})\,(\boldsymbol{\epsilon}_{\mathbf{k}\mu}\cdot\hat{\mathbf{p}}_{-\mathbf{k}})\right\rangle, \tag{12}$$

$$M_{4,\mu}(\mathbf{k}) = \frac{1}{Nm^2}\sum_{\mathbf{ll'}} e^{i\mathbf{k}\cdot(\mathbf{l}-\mathbf{l'})}\left\langle\left(\boldsymbol{\epsilon}_{\mathbf{k}\mu}\cdot\boldsymbol{\nabla}_{\mathbf{l}}\hat{V}\right)\left(\boldsymbol{\epsilon}_{\mathbf{k}\mu}\cdot\boldsymbol{\nabla}_{\mathbf{l'}}\hat{V}\right)\right\rangle$$

$$= \frac{1}{m^2}\left\langle\left(\boldsymbol{\epsilon}_{\mathbf{k}\mu}\cdot\boldsymbol{\nabla}_{\mathbf{k}}\hat{V}\right)\left(\boldsymbol{\epsilon}_{\mathbf{k}\mu}\cdot\boldsymbol{\nabla}_{-\mathbf{k}}\hat{V}\right)\right\rangle, \tag{13}$$

$$M_{6,\mu}(\mathbf{k}) = \frac{1}{N}\frac{1}{m^4}\sum_{\alpha\beta}\epsilon_{\mathbf{k}\mu,\alpha}\epsilon_{\mathbf{k}\mu,\beta}\sum_{\mathbf{ll'}} e^{i\mathbf{k}\cdot(\mathbf{l}-\mathbf{l'})}\sum_{\mathbf{mm'}}\sum_{\gamma\gamma'}\left\{\left\langle\hat{p}_{\mathbf{m}\gamma}\hat{p}_{\mathbf{m'}\gamma'}\frac{\partial^2\hat{V}}{\partial\hat{\boldsymbol{\xi}}_{\mathbf{l}\alpha}\partial\hat{\boldsymbol{\xi}}_{\mathbf{m}\gamma}}\frac{\partial^2\hat{V}}{\partial\hat{\boldsymbol{\xi}}_{\mathbf{l'}\beta}\partial\hat{\boldsymbol{\xi}}_{\mathbf{m'}\gamma'}}\right\rangle\right.$$

$$+i\hbar\left[\left\langle\hat{p}_{\mathbf{m}\gamma}\frac{\partial^3\hat{V}}{\partial\hat{\boldsymbol{\xi}}_{\mathbf{l}\alpha}\partial\hat{\boldsymbol{\xi}}_{\mathbf{m}\gamma}\partial\hat{\boldsymbol{\xi}}_{\mathbf{m'}\gamma'}}\right\rangle + \left\langle\hat{p}_{\mathbf{m'}\gamma'}\frac{\partial^3\hat{V}}{\partial\hat{\boldsymbol{\xi}}_{\mathbf{l}\beta}\partial\hat{\boldsymbol{\xi}}_{\mathbf{m}\gamma}\partial\hat{\boldsymbol{\xi}}_{\mathbf{m'}\gamma'}}\right\rangle\right]$$

$$\left.-\frac{1}{2}\hbar^2\left[\left\langle\frac{\partial^2\hat{V}}{\partial\hat{\boldsymbol{\xi}}_{\mathbf{l}\alpha}\partial\hat{\boldsymbol{\xi}}_{\mathbf{m}\gamma}}\frac{\partial^4\hat{V}}{\partial\hat{\boldsymbol{\xi}}_{\mathbf{l'}\beta'}\partial\hat{\boldsymbol{\xi}}_{\mathbf{m}\gamma}\partial\hat{\boldsymbol{\xi}}_{\mathbf{m'}\gamma'}\partial\hat{\boldsymbol{\xi}}_{\mathbf{m}}}\right\rangle + \frac{1}{2}\left\langle\frac{\partial^3\hat{V}}{\partial\hat{\boldsymbol{\xi}}_{\mathbf{l}\alpha}\partial\hat{\boldsymbol{\xi}}_{\mathbf{m}\gamma}\partial\hat{\boldsymbol{\xi}}_{\mathbf{m}\gamma}}\frac{\partial^3\hat{V}}{\partial\hat{\boldsymbol{\xi}}_{\mathbf{l'}\beta}\partial\hat{\boldsymbol{\xi}}_{\mathbf{m'}\gamma'}p\hat{\boldsymbol{\xi}}_{\mathbf{m'}\gamma'}}\right\rangle\right]\right\}, \tag{14}$$

where we have introduced the notation

$$\boldsymbol{\nabla}_{\mathbf{l}} = \frac{\partial}{\partial\hat{\boldsymbol{\xi}}_{\mathbf{l}}} \tag{15}$$

and

$$\boldsymbol{\nabla}_{\mathbf{k}} = \frac{1}{\sqrt{N}}\sum_{\mathbf{l}} e^{i\mathbf{k}\cdot\mathbf{l}}\boldsymbol{\nabla}_{\mathbf{l}}. \tag{16}$$

In the classical regime the integration over the momenta can be easily carried out so that Eqs. (11)–(14) reduce to

$$M_{0,\mu}(\mathbf{k}) = \left\langle(\boldsymbol{\epsilon}_{\mathbf{k}\mu}\cdot\boldsymbol{\xi}_{\mathbf{k}})\,(\boldsymbol{\epsilon}_{\mathbf{k}\mu}\cdot\boldsymbol{\xi}_{-\mathbf{k}})\right\rangle, \tag{17}$$

$$M_{2,\mu}(\mathbf{k}) = \frac{1}{m\beta}, \tag{18}$$

$$M_{4,\mu}(\mathbf{k}) = \frac{1}{m^2}\left\langle(\boldsymbol{\epsilon}_{\mathbf{k}\mu}\cdot\boldsymbol{\nabla}_{\mathbf{k}}V)\,(\boldsymbol{\epsilon}_{\mathbf{k}\mu}\cdot\boldsymbol{\nabla}_{-\mathbf{k}}V)\right\rangle, \tag{19}$$

$$M_{6,\mu}(\mathbf{k}) = \frac{1}{m^3\beta}\sum_{\mathbf{m}\gamma}\left\langle\left[\frac{\partial}{\partial\boldsymbol{\xi}_{\mathbf{m}\gamma}}(\boldsymbol{\epsilon}_{\mathbf{k}\mu}\cdot\boldsymbol{\nabla}_{\mathbf{k}}V)\right]\right.$$

$$\left.\times\left[\frac{\partial}{\partial\boldsymbol{\xi}_{\mathbf{m}\gamma}}(\boldsymbol{\epsilon}_{\mathbf{k}\mu}\cdot\boldsymbol{\nabla}_{-\mathbf{k}}V)\right]\right\rangle. \tag{20}$$

The angular brackets here denote the classical configurational average

$$\langle A\rangle = \frac{1}{Z_C}\left(\frac{m}{2\pi\hbar^2\beta}\right)^{3N/2}\int d\mathbf{X}A(\mathbf{X})e^{-\beta V(\mathbf{X})}, \tag{21}$$

and the classical partition function reads

$$Z_C = \left(\frac{m}{2\pi\hbar^2\beta}\right)^{3N/2}\int d\mathbf{X}e^{-\beta V(\mathbf{X})}. \tag{22}$$

Therefore the evaluation of the frequency moments in the classical regime can be carried out by means of standard Monte Carlo computations. In the following we shall refer to this procedure by the label CMC (classical Monte Carlo).

III. QUANTUM AVERAGES

In the last section we have seen that the calculation of the frequency moments requires the evaluation of mechanical equilibrium averages such as static correlation functions. In the quantum regime statistical averages of functions of coordinates and conjugate momenta can be expressed as follows:[11]

$$\langle\hat{A}\rangle = \frac{1}{Z}\int d\mathbf{Y}A\left(i\hbar\partial_{\boldsymbol{\eta}}, \mathbf{Y}-\frac{1}{2}\boldsymbol{\eta}\right)$$

$$\times\rho\left(\mathbf{Y}-\frac{1}{2}\boldsymbol{\eta}, \mathbf{Y}+\frac{1}{2}\boldsymbol{\eta}\right)\Big|_{\boldsymbol{\eta}=0}, \tag{23}$$

where $\rho(\mathbf{X}_A, \mathbf{X}_B)$ is the non-normalized density matrix, Z is the partition function, and the function A appearing in the integral is the so-called **p**-left ordered form of the related operator $\hat{A}$.

In the classical regime Eq. (23) reduces to the classical phase space integral which, after the trivial integration over momenta, leads to Eqs. (21) and (22).

An ideal starting point to deal with the quantum statistical average (23) is the path integral formulation of equilibrium statistical mechanics. Within this formalism the density matrix $\rho(\mathbf{X}_A, \mathbf{X}_B)$ is expressed by an integral over all paths $\mathbf{X}(u)$, $u\epsilon[0, \beta\hbar]$, having the initial point $\mathbf{X}(0) = \mathbf{X}_A$ and the final point $\mathbf{X}(\beta\hbar) = \mathbf{X}_B$ so that

$$\rho(\mathbf{X}_A, \mathbf{X}_B) = \int_{\mathbf{X}_A}^{\mathbf{X}_B} D[\mathbf{X}(u)]e^{-S[\mathbf{X}(u)]}, \tag{24}$$

where the weighting factor $S[\mathbf{X}(u)]$ is the Euclidian action defined by

$$S[\mathbf{X}(u)] = \int_0^{\beta\hbar}\frac{du}{\hbar}\left[\frac{m}{2}\dot{\mathbf{X}}^2(u) + V(\mathbf{X}(u))\right]. \tag{25}$$

A. Path-integral Monte Carlo (PIMC)

In the PIMC approach the integration over the "imaginary time" u is approximated by a summation over a discrete set $u_J = \beta\hbar J/P$ with $J = 0, 1, \ldots, P$, where P is called the Trotter number, so that the density matrix appearing in (23) can be written

$$\rho(\mathbf{X}_A, \mathbf{X}_B) = \left(\frac{mP}{2\pi\hbar^2\beta}\right)^{3NP/2} \left[\prod_{J=1}^{P-1} \int d\mathbf{X}_J\right] \exp\left\{-\beta V_{\mathrm{PIMC}}(\{\mathbf{X}_J\})\right\}, \tag{26}$$

where $\mathbf{X}_J \equiv \mathbf{X}(u_J)$ and the potential in the Boltzmann factor is defined by

$$V_{\mathrm{PIMC}}(\{\mathbf{X}_J\}) = \frac{mP}{2\hbar^2\beta^2} \sum_{J=1}^{P} (\mathbf{X}_J - \mathbf{X}_{J-1})^2 - \frac{1}{2P} \sum_{J=1}^{P} [V(\mathbf{X}_J) + V(\mathbf{X}_{J-1})], \tag{27}$$

with $\mathbf{X}_0 = \mathbf{X}_A$ and $\mathbf{X}_P = \mathbf{X}_B$. The averages of observables with a simple dependence on $\mathbf{p}$ can be easily evaluated using the PIMC approximation of the density matrix in Eq. (23);[11] for the first three even moments we have

$$M_{0,\mu} = \left\langle [\boldsymbol{\epsilon}_{\mathbf{k}\mu} \cdot \boldsymbol{\xi}_{\mathbf{k}}(\mathbf{X}_P)] \, [\boldsymbol{\epsilon}_{\mathbf{k}\mu} \cdot \boldsymbol{\xi}_{-\mathbf{k}}(\mathbf{X}_P)] \right\rangle_{\mathrm{PIMC}}, \tag{28}$$

$$M_{2,\mu} = \frac{P}{m\beta} - \frac{1}{N} \frac{P^2}{\hbar^2\beta^2} \sum_{\mathbf{l}\mathbf{l}'} e^{i\mathbf{k}\cdot(\mathbf{l}-\mathbf{l}')} \left\langle [\boldsymbol{\epsilon}_{\mathbf{k}\mu} \cdot (\mathbf{X}_{\mathbf{l}} - \mathbf{X}_P)_{\mathbf{l}}] \, [\boldsymbol{\epsilon}_{\mathbf{k}\mu} \cdot (\mathbf{X}_{\mathbf{l}} - \mathbf{X}_P)_{\mathbf{l}'}] \right\rangle_{\mathrm{PIMC}}, \tag{29}$$

$$M_{4,\mu} = \left\langle [\boldsymbol{\epsilon}_{\mathbf{k}\mu} \cdot \boldsymbol{\nabla}_{\mathbf{k}} V(\mathbf{X}_P)] \, [\boldsymbol{\epsilon}_{\mathbf{k}\mu} \cdot \boldsymbol{\nabla}_{-\mathbf{k}} V(\mathbf{X}_P)] \right\rangle_{\mathrm{PIMC}}, \tag{30}$$

where the contracted notation $\langle\ \rangle_{\mathrm{PIMC}}$ has been introduced for the normalized classical-like configurational integral whose Boltzmann weighting factor is defined in Eqs. (26) and (27). Explicitly, the average of a function $A(\{\mathbf{X}_J\})$ reads

$$\langle A \rangle_{\mathrm{PIMC}} = \frac{1}{Z_{\mathrm{PIMC}}} \left(\frac{mP}{2\pi\hbar^2\beta}\right)^{3NP/2} \left[\prod_{J=1}^{P} \int d\mathbf{X}_J\right] A\left(\{\mathbf{X}_J\}\right) \exp\left\{-\beta V_{\mathrm{PIMC}}\left(\{\mathbf{X}_J\}\right)\right\}, \tag{31}$$

where

$$Z_{\mathrm{PIMC}} = \left(\frac{mP}{2\pi\hbar^2\beta}\right)^{3NP/2} \left[\prod_{J=1}^{P} \int d\mathbf{X}_J\right] \exp\left\{-\beta V_{\mathrm{PIMC}}(\{\mathbf{X}_J\})\right\} \tag{32}$$

and $\mathbf{X}_0 = \mathbf{X}_P$. In view of these expressions the evaluation of the frequency moments within the PIMC approach turns out to involve the calculation of classical-like configuration integrals, but for a system of $N \times P$ particles. Therefore numerical evaluation of these expressions can be set up in the form of standard classical Monte Carlo simulations. However, in order to obtain exact results in the quantum regime ($P \to \infty$) an extrapolation of the numerical outcomes for increasing values of P is necessary. For this reason the PIMC technique is very time consuming in practice, and sometimes provides results that are not completely reliable. Moreover, the accuracy of the calculations becomes worse and worse for increasing Trotter numbers.

B. Effective potential

The effective potential method developed by Giachetti and Tognetti[4–6] is based on a variational approximation for the partition function, and has been successfully used to calculate thermodynamic averages of observables closely related to the free energy and its derivatives.[13–15] Recently this method has been generalized in order to calculate quantum averages of functions of coordinates and conjugate momenta. Cuccoli *et al.*[11,16,12] applied the effective potential method to a linear chain of particles interacting with their nearest neighbors, in order to reconstruct the spectral shape of the displacement correlation function by the evaluation of the related frequency moments. Our aim in this section is to obtain the expressions for the first three even moments for a 3D system.

Let us recall the most important features of the effective potential framework. The density matrix is approximated by

$$\rho(\mathbf{Y} - \tfrac{1}{2}\boldsymbol{\eta}, \mathbf{Y} + \tfrac{1}{2}\boldsymbol{\eta}) = \left(\frac{m}{2\pi\hbar^2\beta}\right)^{3N/2} \int d\mathbf{X}\, e^{-\beta V_G(\mathbf{X})} \prod_{\mathbf{k}\mu} \exp\left[\frac{\lambda_{\mathbf{k}\mu}(\mathbf{X})}{2\hbar^2} \eta_{\mathbf{k}\mu}^2\right] \prod_{\mathbf{k}\mu} \frac{\exp\left[-\frac{(\mathbf{Y}_{\mathbf{k}\mu} - \mathbf{X}_{\mathbf{k}\mu})^2}{2\alpha_{\mathbf{k}\mu}(\mathbf{X})}\right]}{[2\pi\alpha_{\mathbf{k}\mu}(\mathbf{X})]^{\frac{1}{2}}}, \tag{33}$$

where the subscripts refer to the normal mode of vibration $\mathbf{k}\mu$ whose frequency $\omega_{\mathbf{k}\mu}(\mathbf{X})$ is obtained through the transformation $U_{\mathbf{k}\mu,\mathbf{l}\alpha}(\mathbf{X})$ which diagonalizes the frequency matrix

$$\omega^2_{\mathbf{lm},\alpha\beta}(\mathbf{X}) = \frac{1}{m}\left\langle \frac{\partial^2 V}{\partial\xi_{\mathbf{l}\alpha}\partial\xi_{\mathbf{m}\beta}}(\mathbf{X}+\boldsymbol{\nu})\right\rangle_{\mathbf{X}}. \tag{34}$$

Here, the shorthand notation $\langle\,\rangle_{\mathbf{X}}$ has been introduced to define the Gaussian average over the variables $\boldsymbol{\nu}$,

$$\langle f(\boldsymbol{\nu})\rangle_{\mathbf{X}} = \int d\boldsymbol{\nu} f(\boldsymbol{\nu}) \prod_{\mathbf{k}\mu} \frac{\exp\left[-\frac{\boldsymbol{\nu}^2_{\mathbf{k}\mu}}{2\alpha_{\mathbf{k}\mu}(\mathbf{X})}\right]}{[2\pi\alpha_{\mathbf{k}\mu}(\mathbf{X})]^{\frac{1}{2}}}. \tag{35}$$

Moreover, the so-called "global" effective potential reads

$$V_G(\mathbf{X}) = \langle V(\mathbf{X}+\boldsymbol{\nu})\rangle_{\mathbf{X}} - \frac{1}{2}\sum_{\mathbf{ll}'}\sum_{\alpha\beta}\alpha_{\mathbf{ll}',\alpha\beta}(\mathbf{X})\left\langle \frac{\partial^2 V}{\partial\boldsymbol{\xi}_{\mathbf{l}\alpha}\partial\boldsymbol{\xi}_{\mathbf{l}'\beta}}(X+\boldsymbol{\nu})\right\rangle_{\mathbf{X}} + \frac{1}{\beta}\sum_{\mathbf{k}\mu}\ln\left(\frac{\sinh f_{\mathbf{k}\mu}(\mathbf{X})}{f_{\mathbf{k}\mu}(\mathbf{X})}\right), \tag{36}$$

where $f_{\mathbf{k}\mu}(\mathbf{X}) = \beta\hbar\omega_{\mathbf{k}\mu}(\mathbf{X})/2$ and

$$\alpha_{\mathbf{ll}',\alpha\beta}(\mathbf{X}) = \sum_{\mathbf{k}\mu} U_{\mathbf{k}\mu,\mathbf{l}\alpha}(\mathbf{X})U_{\mathbf{k}\mu,\mathbf{l}'\beta}(\mathbf{X})\alpha_{\mathbf{k}\mu}(\mathbf{X}). \tag{37}$$

Finally, the "quantum renormalization parameters" $\alpha_{\mathbf{k}\mu}$ and $\lambda_{\mathbf{k}\mu}$appearing in the preceding equations are defined in terms of the eigenvalues of the frequency matrix (34) as follows:

$$\alpha_{\mathbf{k}\mu}(\mathbf{X}) = \frac{\hbar}{2m\omega_{\mathbf{k}\mu}(\mathbf{X})}\left(\coth f_{\mathbf{k}\mu}(\mathbf{X}) - \frac{1}{f_{\mathbf{k}\mu}(\mathbf{X})}\right), \tag{38}$$

$$\lambda_{\mathbf{k}\mu}(\mathbf{X}) = \frac{m}{\beta} + \gamma_{\mathbf{k}\mu}(\mathbf{X}), \tag{39}$$

where $\gamma_{\mathbf{k}\mu}(\mathbf{X}) = m^2\omega^2_{\mathbf{k}\mu}(\mathbf{X})\alpha_{\mathbf{k}\mu}(\mathbf{X})$. These parameters represent the pure quantum contribution to the quadratic fluctuations of position and momentum of the normal mode $\mathbf{k}\mu$ evaluated in a Gaussian approximation.

The quantum average of observables depending on coordinates and momenta can be obtained by using the effective potential approximation for the density matrix in Eq. (23). Explicit expressions for operators with a simple dependence on $\mathbf{p}$ are given in Ref. 11. Let us recall here the equations we need to calculate the first three even moments, namely,

$$\langle\hat{A}\rangle = \langle\langle A(\mathbf{X}+\boldsymbol{\nu})\rangle_{\mathbf{X}}\rangle_G, \tag{40}$$

$$\langle\hat{p}_{\mathbf{l}\alpha}\hat{p}_{\mathbf{l}'\beta}\rangle = \langle\lambda_{\mathbf{ll}',\alpha\beta}(\mathbf{X})\rangle_G, \tag{41}$$

where $\hat{A}$ is an operator depending on the coordinates only, and

$$\lambda_{\mathbf{ll}',\alpha\beta}(\mathbf{X}) = \sum_{\mathbf{k}\mu} U_{\mathbf{k}\mu,\mathbf{l}\alpha}(\mathbf{X})U_{\mathbf{k}\mu,\mathbf{l}'\beta}(\mathbf{X})\lambda_{\mathbf{k}\mu}(\mathbf{X}). \tag{42}$$

In Eqs. (40) and (41) we have also introduced the notation $\langle\,\rangle_G$ for the classical configurational average with the effective potential:

$$\langle A\rangle_G = \frac{1}{Z_G}\left(\frac{m}{2\pi\hbar^2\beta}\right)^{3N/2}\int d\mathbf{X}A(\mathbf{X})e^{-\beta V_G(\mathbf{X})}, \tag{43}$$

where the partition function Z_G is

$$Z_G = \left(\frac{m}{2\pi\hbar^2\beta}\right)^{3N/2}\int d\mathbf{X}e^{-\beta V_G(\mathbf{X})}. \tag{44}$$

The formalism so far developed is still too complicated to handle because of the implicit dependence on $\mathbf{X}$ in the quantum renormalization parameters and in the frequency matrix (34). To make it computationally tractable, in what follows we will use the low coupling approximation (LCA) in its lowest-order form. In this approximation all the configuration-dependent quantities are expanded around the minimum $\mathbf{X} = \mathbf{X}_0$ of $V_G(\mathbf{X})$, and only first-order terms in $\delta\omega^2_{\mathbf{k}\mu}(\mathbf{X}) = \omega^2_{\mathbf{k}\mu}(\mathbf{X}) - \omega^2_{\mathbf{k}\mu}(\mathbf{X}_0) = \epsilon$ are retained in all the calculations and in the quantum renormalization parameters $\{\alpha\}$. The details of this procedure are extensively described in a previous paper;[11] we outline here only its basic features, and refer the reader to the aforementioned reference for a deeper discussion. The first advantage of the LCA manifests itself in solving the secular equation (34). Due to the translational invariance of the system, the orthogonal matrix $U_{\mathbf{k}\mu,\mathbf{l}\alpha}(\mathbf{X}_0)$ turns into the tensor product of a Fourier transformation and the 3×3 polarization matrix $\epsilon_{\mathbf{k}\mu,\alpha}$. If "bare" frequencies are used, we have simply

$$\omega^2_{\mathbf{k}\mu} = \sum_{\alpha\beta}\epsilon_{\mathbf{k}\mu,\alpha}\omega^2_{\mathbf{k},\alpha\beta}\epsilon_{\mathbf{k}\mu,\beta}, \tag{45}$$

where, for a fcc lattice, the frequency matrix $\omega^2_{\mathbf{k},\alpha\beta}$ can be written

$$\omega^2_{\mathbf{k},\alpha\beta} = \sum_n\sum_{\mathbf{d}_n}\frac{u_{\alpha\beta}(d_n)}{m}2\sin^2\left(\frac{\mathbf{k}\cdot\mathbf{d}_n}{2}\right), \tag{46}$$

where $u_{\alpha\beta}$ is the second derivative tensor of the central potential $u(r)$. Furthermore, by taking advantage of the pairwise form of the interaction potential, the effective potential V_G can now be written in a much more convenient way as follows:

$$V_G(\mathbf{X}) = \frac{1}{2}\sum_{\mathbf{l}}\sum_{n}\sum_{\mathbf{d}_n}\left\{u\left(|\mathbf{x}_{\mathbf{l}+\mathbf{d}_n}-\mathbf{x}_{\mathbf{l}}|\right)+\frac{1}{2}\sum_{\alpha\beta}\left[u_{\alpha\beta}\left(|\mathbf{x}_{\mathbf{l}+\mathbf{d}_n}-\mathbf{x}_{\mathbf{l}}|\right)-u_{\alpha\beta}(d_n)\right]D_{\mathbf{l}\mathbf{d}_n,\alpha\beta}\right\}+\frac{1}{\beta}\sum_{\mathbf{k}\mu}\ln\frac{\sinh f_{\mathbf{k}\mu}}{f_{\mathbf{k}\mu}}, \quad (47)$$

where $D_{\mathbf{l}\mathbf{d}_n,\alpha\beta}$ is the pure quantum part of the square of the displacement between the atom $\mathbf{l}$ and its nth-neighbor shell in the $\mathbf{d}_n$ direction; for a fcc lattice the expression for it reads

$$D_{\mathbf{l}\mathbf{d}_n,\alpha\beta} = \sum_{\mathbf{k}\mu} 4\sin^2\left(\frac{\mathbf{k}\cdot\mathbf{d}_n}{2}\right)\epsilon_{\mathbf{k}\mu,\alpha}\epsilon_{\mathbf{k}\mu,\beta}\alpha_{\mathbf{k}\mu}. \quad (48)$$

The tensor $D_{\mathbf{l}\mathbf{d}_n,\alpha\beta}$ is invariant under operations of the lattice translation group but has a nontrivial dependence on the direction of $\mathbf{d}_n$. However, the calculations can be greatly simplified by assuming that the different components of the relative atom displacements are uncorrelated and the tensorial product appearing in Eq. (47) can be calculated using the approximation

$$\mathrm{vers}(\mathbf{x}_{\mathbf{l}+\mathbf{d}_n}-\mathbf{x}_{\mathbf{l}}) \simeq \mathrm{vers}(\mathbf{d}_n) \equiv \hat{\mathbf{d}}_n, \quad (49)$$

so that

$$\sum_{\alpha\beta} u_{\alpha\beta}(r)D_{\mathbf{l}\mathbf{d}_n,\alpha\beta} \simeq u''(r)D_n^L + \frac{u'(r)}{r}D_n^T. \quad (50)$$

Therefore, only the longitudinal (D_n^L) and transverse projections (D_n^T) of the tensor $\mathbf{D}_n \equiv D_{\mathbf{l}\mathbf{d}_n,\alpha\beta}$ need to be considered, and these parameters are invariant under the operations of the lattice rotation group. At the present stage the expressions for the frequency moments up to the fourth can be obtained by means of the LCA form (first order) of Eqs. (40) and (41), which read

$$\langle A\rangle = \langle A(\mathbf{X})\rangle_G + \frac{1}{2}\sum_{\mathbf{l}\mathbf{l}'}\sum_{\alpha\beta}\alpha_{\mathbf{l}\mathbf{l}',\alpha\beta}\left\langle\frac{\partial^2 A}{\partial x_{\mathbf{l}\alpha}\partial x_{\mathbf{l}'\beta}}(\mathbf{X})\right\rangle_G + \frac{1}{2}\sum_{\mathbf{l}\mathbf{l}'}\sum_{\alpha\beta}\langle\delta\alpha_{\mathbf{l}\mathbf{l}',\alpha\beta}(\mathbf{X})\rangle_G\frac{\partial^2 A}{\partial x_{\mathbf{l}\alpha}\partial x_{\mathbf{l}'\beta}}(\mathbf{X}_0) + O(\alpha\epsilon^2), \quad (51)$$

$$\langle p_{\mathbf{l}\alpha}p_{\mathbf{l}'\beta}\rangle = \frac{m}{\beta}\delta_{\mathbf{l}\mathbf{l}'}\delta_{\alpha\beta} + \gamma_{\mathbf{l}\mathbf{l}',\alpha\beta} + \langle\delta\gamma_{\mathbf{l}\mathbf{l}',\alpha\beta}(\mathbf{X})\rangle_G + O(\alpha\epsilon^2), \quad (52)$$

where the terms $\delta\alpha, \delta\gamma$ take into account the deviation of the renormalization parameters from the exact values calculated on the basis of $\omega(\mathbf{X}_0)$ (to first order in ϵ). The derivation of the frequency moments is then carried out exactly as discussed in Ref. 11 with the slight difference that in our calculations bare frequencies are used. The expressions obtained for the frequency moments up to the fourth are

$$M_{0,\mu}(\mathbf{k}) = \left\langle(\boldsymbol{\epsilon}_{\mathbf{k}\mu}\cdot\boldsymbol{\xi}_{\mathbf{k}})(\boldsymbol{\epsilon}_{\mathbf{k}\mu}\cdot\boldsymbol{\xi}_{-\mathbf{k}})\right\rangle_G + \alpha_{\mathbf{k}\mu} + \frac{1}{2\omega_{\mathbf{k}\mu}}\frac{\partial\alpha_{\mathbf{k}\mu}}{\partial\omega_{\mathbf{k}\mu}}\langle\delta\omega^2_{\mathbf{k}\mu}(\mathbf{X})\rangle_G, \quad (53)$$

$$M_{2,\mu}(\mathbf{k}) = \frac{1}{m\beta} + \alpha_{\mathbf{k}\mu}\omega^2_{\mathbf{k}\mu} + \left(\alpha_{\mathbf{k}\mu} + \frac{\omega_{\mathbf{k}\mu}}{2}\frac{\partial\alpha_{\mathbf{k}\mu}}{\partial\omega_{\mathbf{k}\mu}}\right)\langle\delta\omega^2_{\mathbf{k}\mu}(\mathbf{X})\rangle_G, \quad (54)$$

$$\begin{aligned}M_{4,\mu}(\mathbf{k}) = {}& \frac{1}{m^2}\left\langle(\boldsymbol{\epsilon}_{\mathbf{k}\mu}\cdot\boldsymbol{\nabla}_{\mathbf{k}}V)(\boldsymbol{\epsilon}_{\mathbf{k}\mu}\cdot\boldsymbol{\nabla}_{-\mathbf{k}}V)\right\rangle_G + \frac{1}{m^2 N}\sum_{n}\sum_{\mathbf{l}\mathbf{l}'}e^{i\mathbf{k}\cdot(\mathbf{l}-\mathbf{l}')}\sum_{\mathbf{d}_n\mathbf{d}'_n}(\boldsymbol{\epsilon}_{\mathbf{k}\mu}\cdot\hat{\mathbf{d}}_n)(\boldsymbol{\epsilon}_{\mathbf{k}\mu}\cdot\hat{\mathbf{d}}'_n)\\ &\times\left[D_n^L\left\langle u'''(x_{\mathbf{l}\mathbf{d}_n})u'(x_{\mathbf{l}'\mathbf{d}'_n})\right\rangle_G + D_n^T\left\langle\left(\frac{u''(x_{\mathbf{l}\mathbf{d}_n})}{x_{\mathbf{l}\mathbf{d}_n}}-\frac{u'(x_{\mathbf{l}\mathbf{d}_n})}{x^2_{\mathbf{l}\mathbf{d}_n}}\right)u'(x_{\mathbf{l}'\mathbf{d}'_n})\right\rangle_G\right]\\ &+\alpha_{\mathbf{k}\mu}\omega^4_{\mathbf{k}\mu} + \left(2\alpha_{\mathbf{k}\mu} + \frac{2\alpha_{\mathbf{k}\mu}}{\partial\omega_{\mathbf{k}\mu}}\omega_{\mathbf{k}\mu}\right)\omega^2_{\mathbf{k}\mu}\langle\delta\omega^2_{\mathbf{k}\mu}(\mathbf{X})\rangle_G, \end{aligned} \quad (55)$$

where we have used the shorthand notation $x_{\mathbf{l}\mathbf{d}_n} = |x_{\mathbf{l}+\mathbf{d}_n} - x_{\mathbf{l}}|$. It should be noted that the approximation (49) has been used once again in order to introduce in (55) the expressions for the longitudinal and transverse projections of $\mathbf{D}_n$. Furthermore, the same approximation enables us to express the deviation $\omega_{\mathbf{k}\mu}(\mathbf{X})$ from the exact eigenvalue $\omega_{\mathbf{k}\mu}(\mathbf{X}_0)$ (first order) by

$$\begin{aligned}\delta\omega^2_{\mathbf{k}\mu}(\mathbf{X}) &= \omega^2_{\mathbf{k}\mu}(\mathbf{X}) - \omega^2_{\mathbf{k}\mu}(\mathbf{X}_0)\\ &= \frac{1}{m}\sum_{n}\sum_{\mathbf{l}\mathbf{d}_n}2\sin^2\left(\frac{\mathbf{k}\cdot\mathbf{d}_n}{2}\right)\left[[u''(r)-u''(d_n)](\boldsymbol{\epsilon}_{\mathbf{k}\mu}\cdot\hat{\mathbf{d}}_n)^2 + \left(\frac{u'(r)}{r}-\frac{u'(d_n)}{d_n}\right)[1-(\boldsymbol{\epsilon}_{\mathbf{k}\mu}\cdot\hat{\mathbf{d}}_n)^2]\right]. \end{aligned} \quad (56)$$

Therefore the average $\langle \delta\omega^2_{\mathbf{k}\mu}(\mathbf{X})\rangle_G$ appearing in the preceding equations involves global averages of derivatives of the central potential only.

The evaluation of the frequency moments within the effective potential approach through Eqs. (53)–(55) involves terms equal to the classical ones, except for the replacement of the classical average by the G average, which can be calculated via classical-like Monte Carlo computations. We shall describe this procedure by the label EPMC (effective potential Monte Carlo). Moreover, the same equations require the evaluation of additional purely quantum correction terms which can be evaluated with high accuracy by means of double-precision FORTRAN codes.

On approaching the classical regime ($\beta\hbar\omega \to 0$) the quantum renormalization parameters vanish so that the global averages turn into the classical ones, and the classical expressions for the moments are recovered with the anharmonicity fully taken into account. Of course, in the quantum regime the effective potential approach gives the exact results for a purely quadratic interaction potential; the nonlinear quantum correction terms are evaluated within the LCA (first order) through the approximation (49). Such an approach has proved to be very accurate for the calculation of thermodynamic observables related to the free energy derivatives[14] and for the kinetic energy.[17] Furthermore, the evaluation of the frequency moments in the quantum regime has been successfully performed for LJ chains with the same quantum coupling as in argon. At this stage it is interesting to check the validity of the method for three-dimensional systems. For this reason the results obtained by means of the effective potential method will be compared in the following with the "exact" results of the PIMC simulations.

IV. MODEL POTENTIAL AND MONTE CARLO SIMULATION

The above formalism is applied in this section to a 3D LJ crystal whose Hamiltonian is given by Eqs. (1) and (2) with a pair interaction potential given by

$$u(r) = 4\epsilon\left[\left(\frac{\sigma}{r}\right)^{12} - \left(\frac{\sigma}{r}\right)^{6}\right]. \tag{57}$$

This simple model, through an appropriate choice of the adjustable parameters m, σ, and ϵ, is able to reproduce reasonably the behavior of thermodynamic observables of rare gas solids such as the internal energy, kinetic energy, specific heat, and pressure.[18] Nevertheless, it is well known that the model needs to be improved to calculate physical quantities closely related to the dispersion curves of these solids such as the time-correlation function defined in (3).[18–20] However, as was stated above, the main purpose of this paper is to focus on the reliability of the effective potential approach for the evaluation of the frequency moments of the quantum spectral function (3). Therefore, at this stage we employ the simple LJ 12-6 model with the interaction potential defined in Eq. (57). In the same spirit, only nearest-neighbor interactions have been dynamically taken into account in all the computations; the contribution of the interactions beyond the nearest-neighbor shell has been considered in a "static approximation" in which the instantaneous relative positions of the atoms are replaced by their (classical) equilibrium values. This approximation apparently does not affect the evaluation of the moments of the spectral function (3), but gives an additional temperature-dependent contribution to the average energy and pressure. This procedure allows us to use the all neighbor interaction parameters ϵ and σ of Ref. 18 which give, for the aim of this paper, a reasonable representation of the equation of state of the system and the dispersion curves. The latter are obtained from the solution of Eqs. (45) and (46) where, as a consequence of the above assumptions, the sum over the neighboring shells drops out, and $\mathbf{d}$ runs over the 12 first neighbors only. The model described above allows us to carry out quantum simulations at low temperature and zero pressure with values of the density in very good agreement with the experimental data.[14,17]

In the next section we report numerical results for two different sets of the free parameters ϵ, σ, m reproducing, respectively, solid argon and solid krypton. The quantum behavior of these solids is determined by the "quantum coupling parameter" $\eta = \hbar\Omega/\epsilon$, which is the ratio between the quantum harmonic energy $\hbar\Omega$ [$\Omega^2 = u''(r_{\min})/m$] and the characteristic energy scale ϵ. For the lighter argon ($\eta = 0.223$), the quantum effects are expected to be more important than for krypton ($\eta = 0.123$)

V. MONTE CARLO EVALUATION OF THE FREQUENCY MOMENTS

In Sec. II it has been shown that the evaluation of the frequency moments in both the classical and quantum regimes can be reduced to the calculation of configurational integrals, which can be carried out by means of Monte Carlo simulations. In all these simulations we have used the single-particle version of the METROPOLIS algorithm;[21] namely, in any single move an atom is picked at random and given a uniform random displacement along each of the coordinate directions. The maximum displacement allowed is an adjustable parameter which has been set so as to lead to an acceptance ratio of 30%–50% of the trial moves.

We have implemented algorithms for CMC, EPMC, and PIMC computations which can be used in principle for every wave vector $\mathbf{k}$ in the reciprocal lattice. In these calculations particular care must be taken in the choice of the simulation box size. In fact, the expressions to be evaluated involve thermal averages of Fourier transforms in $\mathbf{k}$ space whose values might be dependent on the box considered if its linear size is not big enough with respect to the wavelength $\lambda = 2\pi/|\mathbf{k}|$. An analysis of the data against the size of the simulation box is sometimes necessary to obtain the correct results in the thermodynamic limit. In practice, if high accuracy is required in the evaluation of the moments, only wave vec-

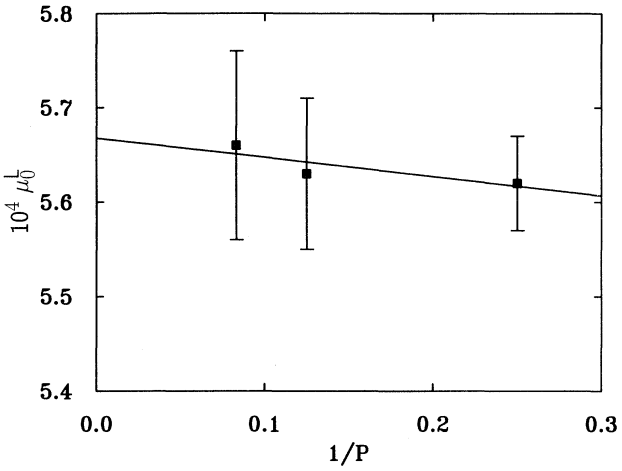

FIG. 1. Longitudinal zeroth moment vs inverse Trotter number P at $T = 20$ K for the wave vector $\mathbf{k} = 2\pi/a_0(1,0,0)$ (boundary zone). The coupling parameter is $\eta = 0.223$ (solid argon). Square box, PIMC data with the harmonic correction (see the text); solid line, extrapolation fit trough points with $P = 4, 8, 12$.

tors at the zone boundary can be investigated by Monte Carlo simulations which, in this case, can be set up with a reasonably small number of particles. The values of the classical and global averages [Eqs. (21) and (43)] involved in the expressions for the frequency moments have been calculated with an error of 0.5% or less by taking the average of 5 independent runs consisting of 10^5 steps per particle. The effective potential expressions for the moments also involve global averages of the central potential derivatives through Eq. (56), whose values turned out to be almost independent of the size of the sample considered and were evaluated with high accuracy by a single run of 10^4 steps per particle using a simulation box of $N = 256$ particles.

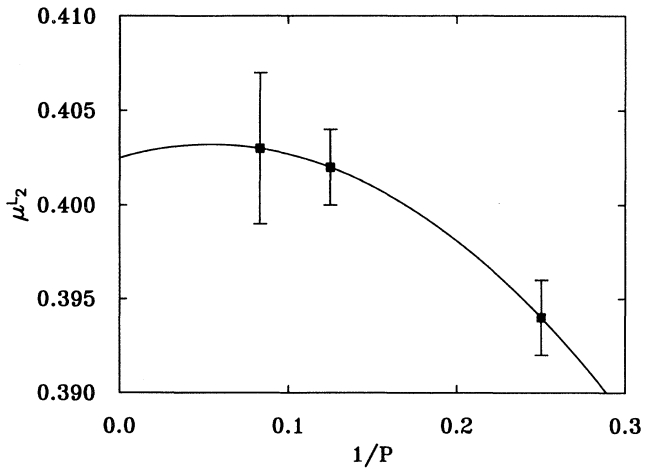

FIG. 2. Longitudinal second moment vs inverse Trotter number P at $T = 20$ K for $\mathbf{k} = 2\pi/a_0(1,0,0)$ and $\eta = 0.223$ (solid argon). Symbols as in Fig. 1.

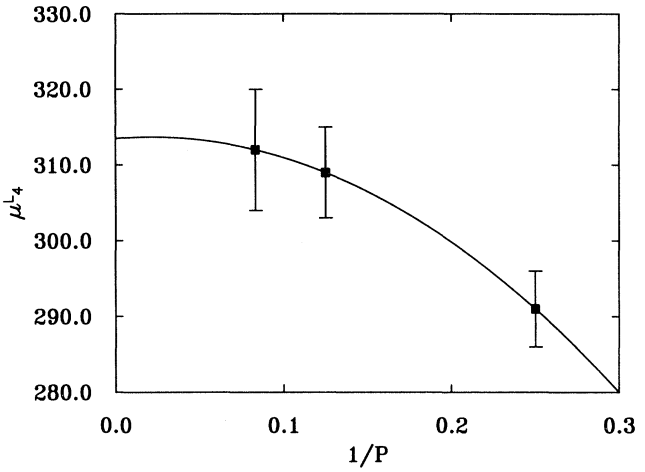

FIG. 3. Longitudinal fourth moment vs inverse Trotter number P at $T = 20$ K for $\mathbf{k} = 2\pi/a_0(1,0,0)$ and $\eta = 0.223$ (solid argon). Symbols as in Fig. 1.

The same box was used in the PIMC simulations and the number P was varied between 4 and 12. Figures 1–3 show how the outcomes of each run have been used to obtain the full quantum mechanical results ($P \to \infty$). All data include the "harmonic correction " extensively described in previous papers,[14,11,17] which consists in adding to the " crude" PIMC outcomes an additional term which is the difference between the exact full quantum result ($P = \infty$) and the finite P result both calculated in the harmonic approximation to the model. Even though this procedure has proved to be very efficient in improving the convergence of the above mentioned extrapolation, the final data are affected by a statistical uncertainty of 5% or more.

VI. NUMERICAL RESULTS AND DISCUSSION

All the data reported in this section are given in dimensionless form by reducing them with respect to the "natural units" of the model; namely, the reduced temperature is defined by $t = kT/\epsilon$, and the moments are measured in units of $\bar{\omega}^{2n}\sigma^2$, where $\bar{\omega} = \sqrt{\epsilon/m\sigma^2}$.

We report below the results for the temperature dependence of the longitudinal and transverse projections of the first four even moments for $\mathbf{k} = (1,0,0)2\pi/a_0$ (in the [100] direction of the reciprocal lattice the transverse modes are degenerate). The results for the zeroth and fourth moments turned out to be unaffected (within the statistical uncertainty) by finite-size effects if a sample consisting of $N = 256$ particles (linear size $L = 4a_0 = 4\lambda$) subjected to periodic boundary conditions was used. The outcomes of both classical and quantum computations refer to the zero-pressure state, so that different values of the density have been used in the two regimes. Figures 4–7 (solid argon) show an excellent agreement in the whole temperature range ($T = 10, 20, 40, 60$ K) between

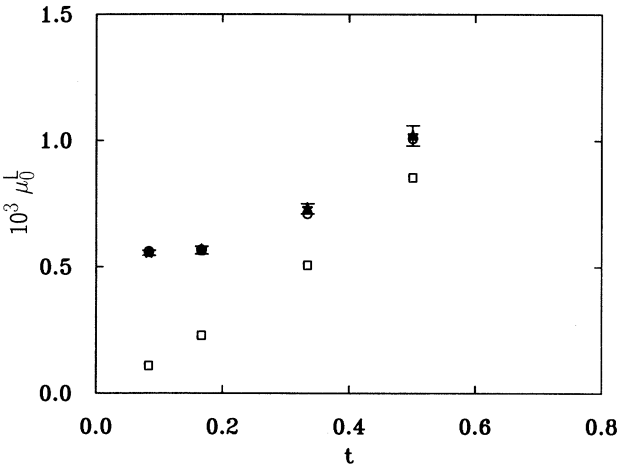

FIG. 4. Temperature dependence of the longitudinal zeroth moment at zero pressure for $\mathbf{k} = 2\pi/a_0(1,0,0)$ and $\eta = 0.223$ (solid argon). Open squares, classical Monte Carlo data (CMC); open circles, effective potential Monte Carlo data (EPMC); stars and error bars, PIMC data.

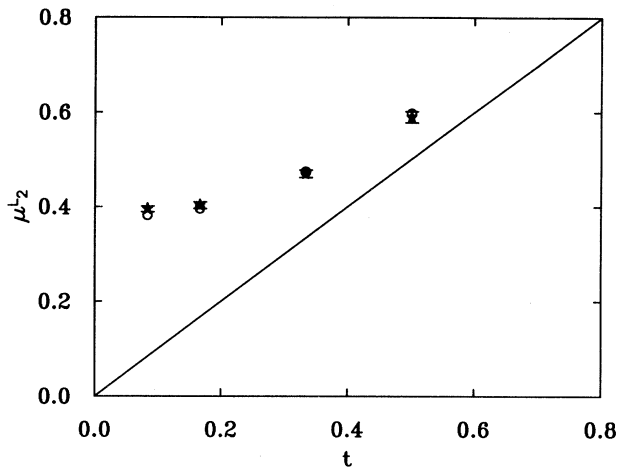

FIG. 6. Temperature dependence of the longitudinal second moment at zero pressure for $\mathbf{k} = 2\pi/a_0(1,0,0)$ and $\eta = 0.223$ (solid argon). Symbols as in Fig. 4 except that the solid line (classical data).

the EPMC and PIMC data for the zeroth and second moments. The situation seems to be a little bit less favorable for the fourth moment (Figs. 8 and 9); even though the reliability of the PIMC data is sometimes questionable we believe that the evaluation of the fourth moment in argon could be slightly underestimated. Since the effect is more visible at low temperatures and for the highest-order moment calculated, the disagreement might be due to a small underestimation of the quantum effects. In other words the effective potential framework based on the lowest-order LCA and on the approximation (49) might fail to take fully into account the quantum anharmonic part of the interaction, which plays an increasingly important role as the order of the moments increases; indeed, higher moments are related to higher-order correlations. For a smaller value of the quantum coupling parameter η (solid krypton) the EPMC and PIMC data match the computational results within the statistical uncertainty, and the agreement is found to be excellent for every moment in the temperature range investigated ($T = 20, 40, 60$ K). Figures 10 and 11 present the data for the fourth moment of krypton.

The evaluation of the sixth moment has been performed in the classical regime only (CMC). At each temperature we have analyzed the data against the size of the box. In particular, different sizes (N from 108 to 4000) have been considered in the simulations, whose results

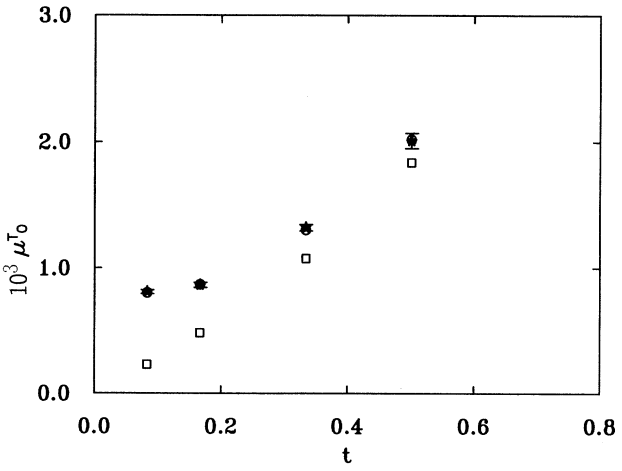

FIG. 5. Temperature dependence of the transverse zeroth moment at zero pressure for $\mathbf{k} = 2\pi/a_0(1,0,0)$ and $\eta = 0.223$ (solid argon). Symbols as in Fig. 4.

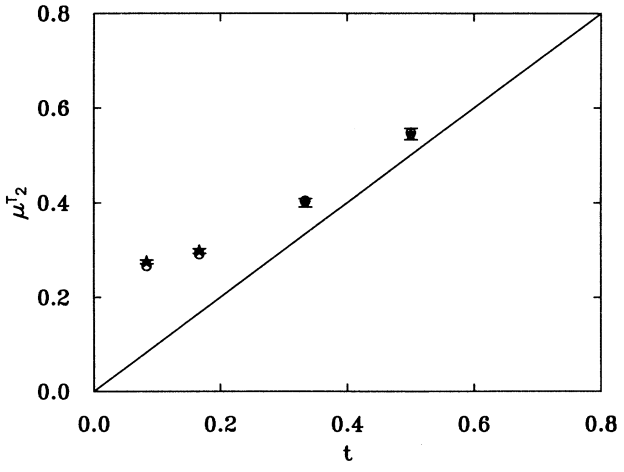

FIG. 7. Temperature dependence of the transverse second moment at zero pressure for $\mathbf{k} = 2\pi/a_0(1,0,0)$ and $\eta = 0.223$ (solid argon). Solid line, classical behavior; open circles, effective potential Monte Carlo data (EPMC); stars and error bars, PIMC data.

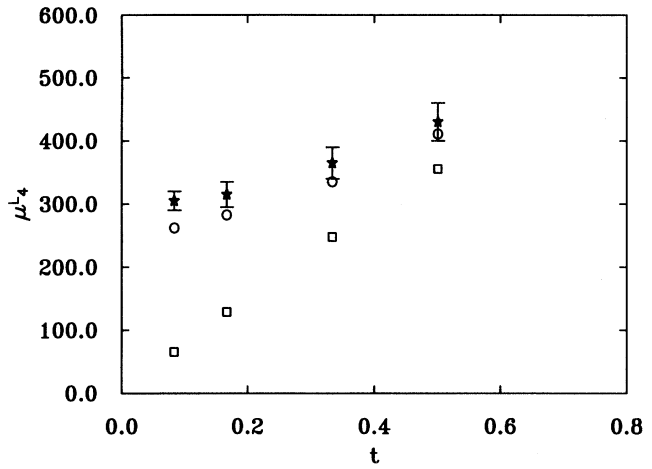

FIG. 8. Temperature dependence of the longitudinal fourth moment at zero pressure for $\mathbf{k} = 2\pi/a_0(1,0,0)$ and $\eta = 0.223$ (solid argon). Symbols as in Fig. 4.

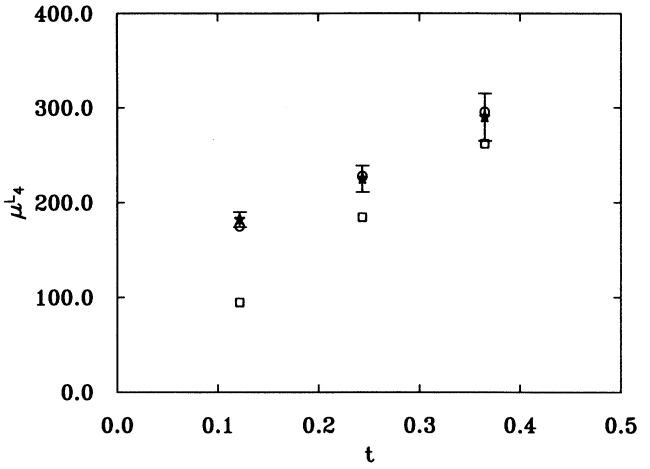

FIG. 10. Temperature dependence of the longitudinal fourth moment at zero pressure for $\mathbf{k} = 2\pi/a_0(1,0,0)$. The coupling parameter is $\eta = 0.123$ (solid krypton). Symbols as in Fig. 4.

have been plotted versus the inverse of the linear size of the box; an example of this procedure is reported in Fig. 12. The same figure shows that the results obtained with the biggest box can be considered a very good approximation to the thermodynamic limit value ($N \to \infty$). Finally, Fig. 13 shows the temperature dependence of the sixth moment (argon), whose thermodynamic limit values are deduced by the aforementioned procedure. We believe this analysis necessary if a statistical error of 1% or less is desired in the calculation of the moments.

VII. CONCLUSIONS

We have presented a detailed description of the techniques available for calculating the frequency moments of the atomic displacements time correlation function of a 3D crystal. We have tested the computations against finite-size effects for wave vectors at the zone boundary of the FBZ. In general, we believe that the first three even moments are unaffected by these effects if the computations are set up respecting the safe condition $L \simeq 8\pi/|\mathbf{k}|$ for the choice of the linear size L of the simulation box. If high accuracy is necessary, we also believe that an analysis of the data as functions of the size of the box is appropriate in calculations of higher moments, which require the evaluation of sums over larger clusters of particles. Finite-size effects increase with the number of shells of neighbors taken dynamically into account in the computations, and turn out to be more important at high temperatures where the configurational phase space is explored more effectively.

We have also developed a method to calculate the frequency moments in the quantum regime for an all neighbors interacting crystal. The numerical data reported

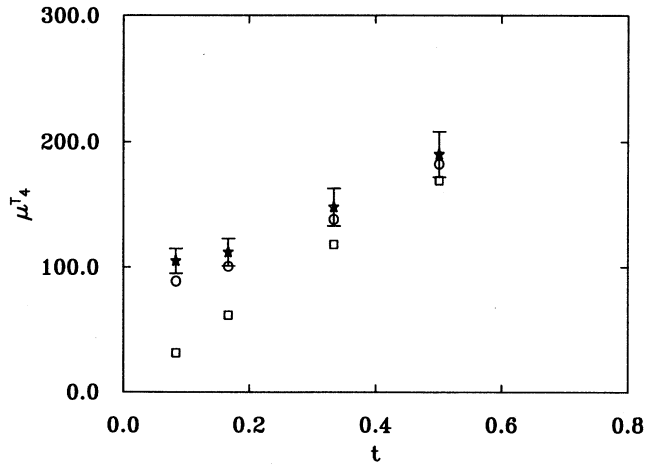

FIG. 9. Temperature dependence of the transverse fourth moment at zero pressure for $\mathbf{k} = 2\pi/a_0(1,0,0)$ and $\eta = 0.223$ (solid argon). Symbols as in Fig. 4.

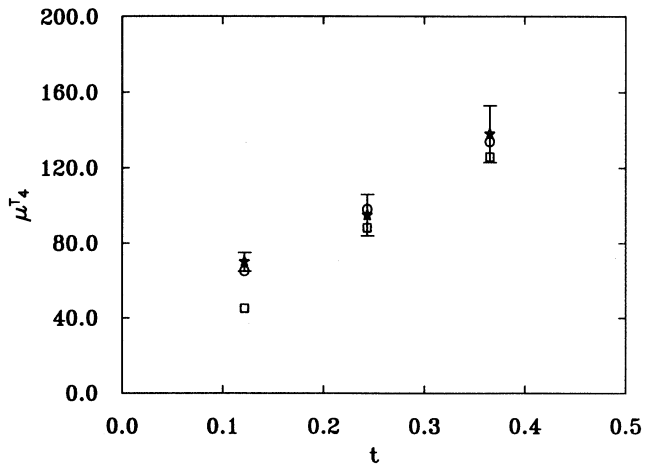

FIG. 11. Temperature dependence of the transverse fourth moment at zero pressure for $\mathbf{k} = 2\pi/a_0(1,0,0)$. The coupling parameter is $\eta = 0.123$ (solid krypton). Symbols as in Fig. 4.

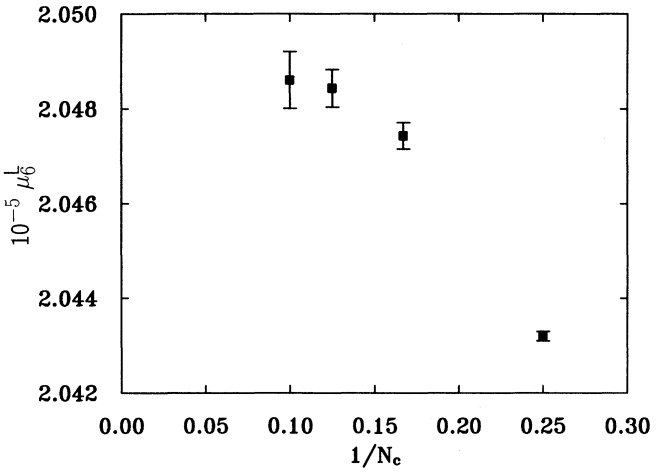

FIG. 12. Longitudinal sixth moment (classical data) vs number of cells per edge of the simluation box for $\mathbf{k} = 2\pi/a_0(1,0,0)$ at $T = 60$ K (argon).

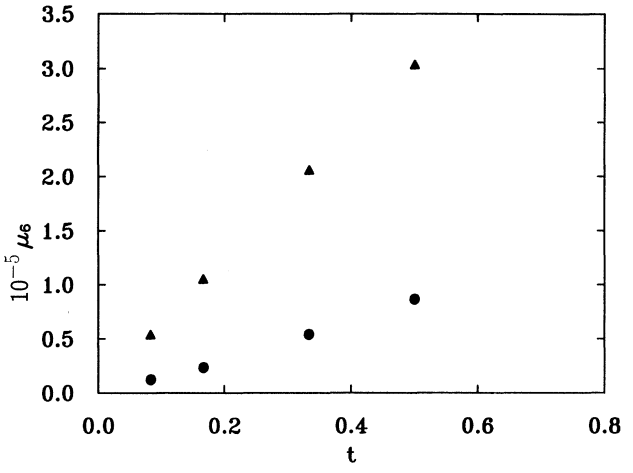

FIG. 13. Temperature dependence of the longitudinal (triangles) and transverse (circles) sixth moment at zero pressure in the classical regime for $\mathbf{k} = 2\pi/a_0(1,0,0)$ (argon).

here refer to a nearest-neighbor potential with a static long-range correction; tests against the extensive PIMC computations show that, for both values of the quantum coupling parametrs η considered here, the effective potential method provides excellent results for the second and the zeroth moments. The latter can be related to the integrated intensity in a neutron scattering experiment which, in the quantum regime, is strongly affected by the zero-point motion of the system.

The limits of our approach show up in the few percent underestimation of the fourth moment in solid argon, but we believe that the method is absolutely reliable for solids with smaller quantum coupling parameters η (krypton, xenon). In this case the advantage of the effective potential method over PIMC resides in the high accuracy which can be achieved in the computations.

It is not an easy task to extend, in a simple form, the formalism developed here beyond the LCA;[22] we believe that efforts to make the method reliable in systems where quantum effects are more important must focus on the possibility of taking into account higher-order terms in the renormalization parameters $\{\alpha\}$. The first step in this direction is allowing the frequency to be renormalized by Eq. (34).[11] Moreover, even though the approximation (49) greatly simplifies the formalism, it might become poor as the order of the moments increases, so that its use in calculating higher moments might be questionable.

Nevertheless, from a knowledge of the first three even moments it is possible to determine the short-time behavior of the atomic displacements time correlation function, and by introducing appropriate approximations for the long-time behavior[23] we believe that an estimate of the phonon lifetimes can be achieved in regions where perturbative methods are no longer valid.[12] This method should be particularly useful in the quantum regime where molecular dynamics simulations are not able to give a correct description of the correlations in the particles' motion. Furthermore, through an appropriate choice of the pair interaction potential, the method could be used throughout a wide temperature range in order to determine the phonon lines shapes of real rare gas crystals that are directly accessible by experimental measurements.

ACKNOWLEDGMENTS

The work of A.A.M. was supported in part by NSF Grant No. DMR 93-19404. This research was also supported by the University of California, Irvine, through an allocation of computer time.

[1] R.P. Feynman, *Statistical Mechanics* (Benjamin, Reading, MA, 1972).
[2] D. Chandler and P.G. Wolynes, J. Chem. Phys. **74**, 4078 (1981).
[3] B.J. Berne and D. Thirumalai, Annu. Rev. Phys. Chem. **37**, 401 (1986).
[4] R. Giachetti and V. Tognetti, Phys. Rev. Lett. **55**, 912 (1985).
[5] R. Giachetti and V. Tognetti, Phys. Rev. B **33**, 7647 (1986).
[6] R. Giachetti and V. Tognetti, J. Magn. Magn. Mater. **54-57**, 861 (1986).
[7] S.W. Lovesey, *Condensed Matter Physics: Dynamic Correlations* (Benjamin/Cummings, Reading MA, 1986).
[8] H. Mori, Prog. Theor. Phys. **33**, 423 (1965).
[9] H. Mori, Prog. Theor. Phys. **34**, 399 (1965).

[10] K. Tomita and H. Tomita, Prog. Theor. Phys. **45**, 1407 (1971).
[11] A. Cuccoli, A.A. Maradudin, A.R. McGurn, V. Tognetti, and R. Vaia, Phys. Rev. B **46**, 8839 (1992).
[12] A. Cuccoli, A.A. Maradudin, A.R. McGurn, V. Tognetti, and R. Vaia, Phys. Rev. B **48**, 7015 (1993).
[13] A. Cuccoli, V. Tognetti, and R. Vaia, Phys. Rev. B **41**, 9588 (1990).
[14] A. Cuccoli, A. Macchi, M. Neumann, V. Tognetti, and R. Vaia, Phys. Rev. B **45**, 2088 (1992).
[15] S. Liu, G.K. Horton, and E.R. Cowley, Phys. Lett. A **152**, 79 (1991).
[16] A. Cuccoli, M. Spicci, V. Tognetti, and R. Vaia, Phys. Rev. B **47**, 7859 (1993).
[17] A. Cuccoli, A. Macchi, V. Tognetti, and R. Vaia, Phys. Rev. B **47**, 14923 (1993).
[18] *Rare Gas Solids*, edited by M.L. Klein and J.A. Venables (Academic Press, London, 1976).
[19] E.R. Cowley and M. Nordberg, Phys. Rev. B **45**, 2493 (1992).
[20] M.L. Klein, J.A. Barker, and T.R. Koehler, Phys. Rev. B **4**, 1983 (1971).
[21] M.P. Allen and D.J. Tildesley, *Computer Simulation of Liquids* (Clarendon Press, Oxford, 1987).
[22] G. Pedrolli (private communication).
[23] H. Tomita and H. Mashiyama, Prog. Theor. Phys. **48**, 1133 (1972).